Non-iterative Robust Economic Dispatch for Interconnected Grids Based on Tie-line Power Transfer Regulation

Yuejian Wu, Xiaoming Dong, Tianguang Lu, Zhengqi Liu, and Chengfu Wang

***Abstract*—The coordinated dispatch of interconnected grids characterized by maldistributed sustainable energy encounters challenges with regional privacy. Thus, this study proposes a non-iterative robust economic dispatch method for interconnected grids based on tie-line power transfer regulation. The economic dispatch model with uncertainties is transformed into a two-layer robust model and further treated as a single-layer linear model by strong duality theorem. Then, the intra-regional submodules are established by temporal and spatial decomposition to enable parallel execution. The inter-regional power transfer feasible region (PTFR) and intra-regional operation cost feasible region (OCFR) are evaluated using multi-parameter programming theory to protect the private and sensitive information of each region and to ensure cost efficiency of dispatch results. Additionally, the boundaries of feasible regions are adjusted by the conservatism budget to address multiple fluctuation intervals of stochastic factors. Finally, the information of feasible regions is shared between each intra-regional operator along with central coordination layer, generating feasible regions of joint economic dispatch along with inter-regional power transfer constraints. The intra-regional dispatch strategy could be rapidly obtained following the decision-making of inter-regional dispatch by mapping relations. Case studies by three modified IEEE test systems demonstrate the preciseness and effectiveness of the proposed method.**

***Index Terms*—Interconnected grid, privacy security, economic dispatch, feasible region, tie-line, power transfer, multi-parameter programming.**

I. Introduction

THE development of electricity market creates the need of establishing multiple independent grids, which realizes decentralized regulation and sufficient competition. Meanwhile, with high penetration of stochastic and unevenly distributed renewable energy sources integrated into power grid, a single system is incapable and uneconomic to solve challenges with its own resources [1]. The existence of tie-lines enables power grids to exchange electric power with others, which provides an opportunity to exchange renewable energy generation with diverse temporal and spatial characteristics [2]-[4]. Through the interconnection of multiple grids, power source and load can be complemented and balanced over a wide range, and system security and flexibility can be enhanced [5], [6].

However, equitable and efficient coordination of interconnected grids has essential obstacles. The operation of interconnected grids is served by independent system operators (ISOs), where information privacy protection is required due to diverse attribution of grids [7]. To mitigate economy and security risks of subordinate grids due to unreasonable power transfer schemes [8], ISOs should consider the potential flexibility of the system in a global perspective for achieving resource complementation. An ideally centralized framework for joint economic dispatch (JED) [9], [10] could facilitate optimal cooperation among multiple grids. However, it necessitates the sharing of private information involving transmission lines, generation units, and loads within each region, which cannot be applied to realize coordinated dispatch among diverse ISOs. A typical solution is to construct distributed framework based on mathematical decomposition methods such as optimal conditional decomposition [11], analytical target cascading [12], alternating direction method of multipliers [13], or indirectly construct critical region (CR) projection [14] through multi-parameter quadratic programming theory. These studies usually entail decomposing a master problem into sub-problems, which are independently addressed by regional ISOs, and the optimality of the dispatch strategy can be guaranteed through either incorporating iterative exchanges of local computation results among regions or establishing a coordination layer.

Under a distributed framework, information privacy is inherently safeguarded, and parallel execution can be deployed for acceleration. However, the convergence and accuracy cannot be guaranteed due to the factors such as communication capability, iteration sequence, and hyperparameter selection. To alleviate communication burden due to repetitive processes, non-iterative distributed framework based on the regional equivalence model has been presented for improve-

Manuscript received: November 21, 2024; revised: February 21, 2025; accepted: April 23, 2025. Date of CrossCheck: April 23, 2025. Date of online publication: September 5, 2025.

This work was supported by the National Natural Science Foundation of China (No. U22B20102).

Y. Wu, X. Dong (corresponding author), T. Lu, and C. Wang are with the School of Electrical Engineering, Shandong University, Jinan 250061, China (e-mail: wuyuejiansdu@163.com; dongxiaoming@sdu.edu.cn; tlu@sdu.edu.cn; wangcf@sdu.edu.cn).

Z. Liu is with State Grid Changsha Power Supply Company, Changsha 410023, China (e-mail: 15927112029@163.com).

DOI: 10.35833/MPCE.2025.000150

ment. Reference [15] proposes a market clearing model among multiple regions, but it is limited to address the single period problem, whereas time coupling is further incorporated in [16]. The performance of tie-lines in terms of AC and DC is discussed in [17] and [18]. A compact form of system representation is proposed in [19] by eliminating redundant constraints and variables effectively. The feasible region of tie-line injections is established in [20] based on the projection theory, specifying the feasible range of the tie-line while ensuring regional security constraints. The model proposed in [21] comprehensively utilizes the implicit flexibility of the regional grids. The aforementioned studies illustrate the effectiveness of the model in addressing the coordinated dispatch for interconnected grids in deterministic scenarios. However, the solutions to dealing with uncertainty factors within the equivalence model deserves further integration, particularly in cases involving increasing penetration of renewable energy generation [22], [23]. In other words, extending existing non-iterative coordination schemes into uncertain optimal dispatch methods is a crucial problem to be solved. As a result, this study proposes the improved models and methods to treat the above issues with the primary contributions summarized as follows.

1) A non-iterative economic dispatch method based on inter-regional power transfer feasible region (PTFR) and the intra-regional operation cost feasible region (OCFR) is proposed.

2) Non-iterative coordination schemes for multi-area economic dispatch are extended to uncertain optimal dispatch methods through robust technique.

3) Private and sensitive information consisting of internal information and robust optimization preferences are protected in PTFR and OCFR.

II. Formulations of JED Model

To safeguard the security and enhance the economic efficiency of power dispatch, the dispatch strategies for intra-regional units and inter-regional power exchanges are based on JED model that utilizes the DC power flow method. The objective function of JED model, given by (1) and (2), describes the overall cost across multiple time periods and regions. Across all time periods and regions, JED model is subject to local constraints in (3)-(12) and inter-regional constraints in (13)-(16). Network security constraints are represented in (3)-(5), where (3) denotes bus power injection, (4) denotes branch power flow constraint, and (5) denotes power balance constraint. Unit operation constraints are described by relations in (7)-(10), where unit capacity constraint is denoted by (6), ramping constraints are denoted by (7) and (8), and interruptible load constraints are denoted by (9) and (10). Renewable energy output constraints are denoted by (11) and (12). Power transfer constraints are denoted by (13)-(16), where the constraint on the total tie-line power within the dispatch time span is denoted by (13), the limits on the tie-line transfer capacity are denoted by (14), the ramping constraint of the tie-line transfer power is denoted by (15), and the bounds on the tie-line transfer power within an allowable range are denoted by (16).

$$F=\min \sum_{a\in \Phi_A}\sum_{t\in \Phi_T} f_t^a \tag{1}$$

$$f_t^a=\sum_{i\in \Phi_G^a} C_{G,i,t}^a P_{G,i,t}^a+\sum_{i\in \Phi_{DR}^a}\sum_{s\in \Phi_S^a} C_{DR,i,t,s}^a P_{DR,i,t,s}^a \tag{2}$$

$$P_{In,i,t}^a=\sum_{\substack{b\in \Phi_A\\ b\neq a}} P_{TL,i,t}^{ab}+P_{G,i,t}^a+P_{RE,i,t}^a-P_{L,i,t}^a+P_{DR,i,t}^a \quad \forall i\in \Phi_N^a, \forall t\in \Phi_T \tag{3}$$

$$\underline{P}_{flow}^a\le G_{l-i}^a P_{In,i,t}^a\le \bar{P}_{flow}^a \quad \forall i\in \Phi_N^a, \forall l\in \Phi_{Lines}^a, \forall t\in \Phi_T \tag{4}$$

$$P_{In,i,t}^a=\sum_{l\in \Phi_{Lines,j}^{From,a}} G_{l-j}^a P_{In,i,t}^a-\sum_{l\in \Phi_{Lines,j}^{To,a}} G_{l-i}^a P_{In,i,t}^a \quad \forall i\in \Phi_N^a, \forall l\in \Phi_{Lines}^a, \forall t\in \Phi_T \tag{5}$$

$$U_{G,i,t}^a \underline{P}_{G,i,t}^a\le P_{G,i,t}^a\le U_{G,i,t}^a \bar{P}_{G,i,t}^a \quad U_{G,i,t}^a\in\{0,1\}, \forall i\in \Phi_G^a, \forall t\in \Phi_T \tag{6}$$

$$P_{G,i,t}^a-P_{G,i,t+1}^a\le P_{Gdown,i}^a U_{G,i,t+1}^a+\frac{1}{2}(1-U_{G,i,t+1}^a)(\underline{P}_{G,i}^a+\bar{P}_{G,i}^a) \quad \forall i\in \Phi_G^a, \forall t,t+1\in \Phi_T \tag{7}$$

$$P_{G,i,t+1}^a-P_{G,i,t}^a\le P_{Gup,i}^a U_{G,i,t}^a+\frac{1}{2}(1-U_{G,i,t}^a)(\underline{P}_{G,i}^a+\bar{P}_{G,i}^a) \quad \forall i\in \Phi_G^a, \forall t,t+1\in \Phi_T \tag{8}$$

$$0\le P_{DR,i,t,s}^a\le\{\lambda_s^a\}P_{L,i,t}^a \quad \forall i\in \Phi_{DR}^a, \forall t\in \Phi_T, \forall s\in \Phi_S^a \tag{9}$$

$$P_{DR,i,t}^a=\sum_{s\in \Phi_S^a} P_{DR,i,t,s}^a \quad \forall i\in \Phi_{DR}^a, \forall t\in \Phi_T \tag{10}$$

$$\sum_{j\in \Phi_{NRE,i}^a} P_{RE,i,j,t}^a\le \sum_{j\in \Phi_{NRE,i}^a}\{P_{PRE,i,j,t}^a\} \quad \forall i\in \Phi_{RE}^a, \forall t\in \Phi_T \tag{11}$$

$$P_{RE,i,t}^a=\sum_{k\in \Phi_{NRE,i}^a} P_{RE,i,k,t}^a \quad \forall i\in \Phi_{RE}^a, \forall t\in \Phi_T \tag{12}$$

$$P_{TL}^{ab}=\sum_{t\in \Phi_T} P_{TLi,t}^{ab} \quad \forall a,b\in \Phi_A \tag{13}$$

$$\underline{P}_{TL,i,j}^{ab}\le P_{TLi,j,t}^{ab}\le \bar{P}_{TL,i,j}^{ab} \quad (i,j)\in \Phi_{NTL}^{ab}, \forall a,b\in \Phi_A, \forall t\in \Phi_T \tag{14}$$

$$PD_{TL}^{ab}\le\sum_{(i,j)\in \Phi_{NTL}^{ab}}(P_{TLi,t}^{ab}-P_{TLi,t-1}^{ab})\le PU_{TL}^{ab} \quad i\in \Phi_{NTL}^{ab}, \forall a,b\in \Phi_A, \forall t\in \Phi_T \tag{15}$$

$$\frac{(1-\sigma)P_{TL}^{ab}}{|\Phi_T|}\le\sum_{(i,j)\in \Phi_{NTL}^{ab}} P_{TLi,t}^{ab}\le\frac{(1+\sigma)P_{TL}^{ab}}{|\Phi_T|} \quad i\in \Phi_{NTL}^{ab}, \forall a,b\in \Phi_A, \forall t\in \Phi_T \tag{16}$$

where a and b are the indexes of regions; Φ_A is the set of regions; t and Φ_T are the index and set of dispatch periods, respectively; i is the index of buses; Φ_N^a is the set of buses; Φ_G^a is the set of generator buses; Φ_{DR}^a is the set of interruptible load buses; s and Φ_S^a are the index and set of interruptible load levels, respectively; k and $\Phi_{NRE,i}^a$ are the index and set of renewable energy at bus i, respectively; Φ_{RE}^a is the set of renewable energy buses; Φ_{Lines}^a is the set of lines; $\Phi_{Lines,j}^{From,a}$ is the set of lines with the beginning bus j; $\Phi_{Lines,j}^{To,a}$ is the set of lines with the ending bus j; Φ_{NTL}^{ab} is the set of the tie-line buses between regions a and b; $C_{G,i,t}^a$ is the generator cost coefficient; $C_{DR,i,t,s}^a$ is the interruptible load cost coefficient; $P_{G,i,t}^a$ is the generator output power; $P_{In,i,t}^a$ is the bus injected

power; $P^{ab}_{TL,i,t}$ is the tie-line transfer power between regions a and b; $P^{a}_{RE,i,t}$ is the renewable energy output; $P^{a}_{L,i,t}$ is the load power; $P^{a}_{DR,i,t}$ is the total interruptible load; $\bar{P}^{a}_{flow}$ and $\underline{P}^{a}_{flow}$ are the upper and lower limits of line capacity, respectively; G^{a}_{l-i} and G^{a}_{l-j} are the power transfer distribution factors from bus i to line l and bus j to line l, respectively; $U^{a}_{G,i,t}$ is the generator operation status, which derives from unit comment results of each region; $\underline{P}^{a}_{G,i,t}$ and $\bar{P}^{a}_{G,i,t}$ are the lower and upper limits of generator capacities, respectively; $P^{a}_{Gdown,i}$ and $P^{a}_{Gup,i}$ are the generator ramp-down and ramp-up rates, respectively; λ_s is the interruption level coefficient; $\{\cdot\}$ denotes the stochastic variable; $P^{a}_{RE,i,j,t}$ is the j^{th} renewable energy output at bus i; $P^{a}_{PRE,i,j,t}$ is the forecast value of the j^{th} renewable energy output at bus i; P^{ab}_{TL} is the total transfer power between regions a and b; $\underline{P}^{ab}_{TL,i,j}$ and $\bar{P}^{ab}_{TL,i,j}$ are the lower and upper limits of line capacity between regions a and b, respectively; PD^{ab}_{TL} and PU^{ab}_{TL} are the ramp-down and ramp-up rates of tie-lines between regions a and b, respectively; and σ is the fluctuation rate control parameter.

When the JED model within a centralized method is solved, several challenges emerge. On one hand, (9) and (11) involve stochastic variables, which introduce uncertainties into the model, making commercial solvers no longer applicable. On the other hand, $P^{ab}_{TL,i,t}$ gives rise to the coupling relationship for different regions. However, due to privacy restrictions on grid data, the absence of a mechanism in inter-regional data access disables any individual grid to confirm these coupling constraints. Furthermore, temporal associations in JED model induced by (7) and (8) elevate the complexity of the model and the difficulty in solving it. Therefore, in the next section, a non-iterative robust economic dispatch method is formulated to tackle issues including model stochasticity, privacy concerns, and complexity.

III. Non-iterative Robust Economic Dispatch Method

The structure of the proposed method is shown in Fig. 1. The optimization process, considering the treatments of stochasticity and privacy, converges to obtain the same results by the traditional centralized JED method. Each region formulates a region-specific dispatch model consisting of PTFR and OCFR. PTFR characterizes the tie-line power transfer capacity restricted by the internal resource ramping capability during adjacent time periods. OCFR represents the specified intra-regional power grid operation cost of inter-regional power transfer scheme, lower bound of which is the optimal operation cost. Using coupling variables as boundaries, PTFR and OCFR present the external characteristics of each region, based on which an optimized power transfer scheme allowing for inter-regional constraints is formulated without relying on a fully shared information mechanism, thereby ensuring the privacy protection of individual grids. Finally, the obtained results are fed back to each region, and power transfer scheme is transformed into intra-regional dispatch strategies for adjusting system resources through mapping relation.

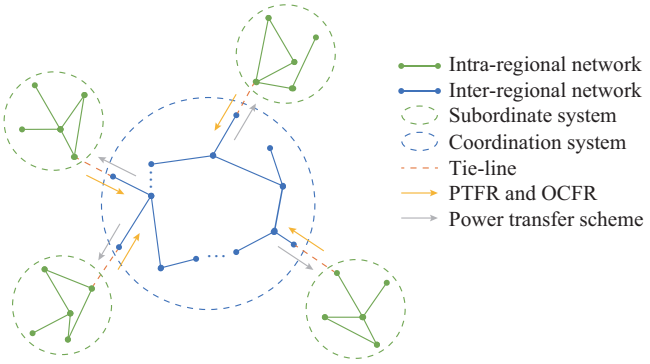

Fig. 1. Structure of proposed method.

A. Sub-model Generation

Owing to the temporally coupled feature of (7) and (8), feasible regions cannot be characterized within a single time period. Considering the entire dispatch period, the dimension of PTFR is sufficiently high. FR^{a}_{PT} is a $|\Phi_T|$-dimensional polyhedron ($FR^{a}_{PT} \subset R^{|\Phi_T|}$), rendering direct quantification unfeasible. Accordingly, the original full-cycle coupled model (considering all constraints during the entire dispatch time span simultaneously in set Φ_T) is decomposed into $|\Phi_T - 1|$ neighboring temporal coupled models (considering constraints within two neighboring time periods), where the PTFR in the original model is the intersection of PTFR in all neighboring temporal coupled models. FR^{a}_{PT} can be co-characterized by $FR^{a}_{PT,t}$ ($t = 1, 2, \ldots, |\Phi_T - 1|$) derived from neighboring temporal coupled models. For $\forall t, t+1 \in \Phi_T$, the neighboring temporal coupled model is given by:

$$\begin{cases} \min(f^{a}_{t} + f^{a}_{t+1}) \\ \text{s.t. } (3)\text{-}(12) \end{cases} \tag{17}$$

The PTFR can be expressed as:

$$FR^{a}_{PT,t} = \{[P^{ab}_{TL,i,t} \quad P^{ab}_{TL,i,t+1}]^{\mathrm{T}} | (3)\text{-}(12)\} \tag{18}$$

Furthermore, since the direction of power flow carried by tie-lines connecting regions a and b could be arbitrary, the relations in (19) and (20) must be satisfied simultaneously.

$$[P^{ab}_{TL,i,t} \quad P^{ab}_{TL,i,t+1}]^{\mathrm{T}} \in FR^{a}_{PT,t} \quad \forall t, t+1 \in \Phi_T \tag{19}$$

$$[-P^{ab}_{TL,i,t} \quad -P^{ab}_{TL,i,t+1}]^{\mathrm{T}} \in FR^{b}_{PT,t} \quad \forall t, t+1 \in \Phi_T \tag{20}$$

The feasibility of intra-regional power grid dispatch is guaranteed by the constraints (18)-(20). Meanwhile, it is essential to quantify the dispatch costs associated with tie-line power transfer to assess the economic performance of the dispatch strategy. According to (2), the dispatch costs of the system encompass both the operation expenses incurred by generation units and the compensation costs associated with interruptible loads, which are directly correlated with unit output and interrupted load management. Therefore, a single-period model for $\forall t \in \Phi_T$ is established as expressed by (21), where the auxiliary variable Z^{a}_{t} and positive constant M_{Const} are introduced to relax the objective solution.

$$\begin{cases}\min Z_t^a \\ \text{s.t. (3)-(6), (9)-(12)} \\ \quad 0 \le Z_t^a - f_t^a \le M_{Const}\end{cases} \tag{21}$$

The feasibility of temporal domain dispatch strategies has been ensured by (18)-(20), and removing constraints (7) and (8) effectively reduces the dimensionality of the model, thereby enhancing the efficiency of subsequent solving process. OCFR can be formulated as:

$$FR_{OC,t}^a = \{[P_{TL,i,t}^{ab} \quad Z_t^a]^{\mathrm{T}} | (3)\text{-}(6),\ (9)\text{-}(12), 0 \le Z_t - f_t^a \le M_{Const}\} \tag{22}$$

With the object of minimizing cost, Z_t^a equals f_t^a when the lower bound of OCFR is reached. The relaxation of constraints can effectively enhance the feasibility of completing multi-parameter optimization, without causing solution errors.

Once the tie-line transfer power is determined, JED could be decoupled into independent economic dispatch models of subordinate grids, which can be directly solved. Nevertheless, (18) and (22), obtained from (17) and (21), respectively, necessitate further supplementation of information such as unit details, loads, and topology. Therefore, a more concise model of (18) and (22) is packaged based on the classical multi-parameter programming theory.

B. Model Packaging

Both (17) and (21) are subject to stochastic linear programming problems. Parameters vary across different time periods and regions, which result in a total of $|\Phi_A||\Phi_T - 1|$ models for (17) and $|\Phi_A||\Phi_T|$ models for (21). The formulations could be collectively simplified as:

$$\begin{cases}\min z = \boldsymbol{\kappa}^{\mathrm{T}} \boldsymbol{x} \\ \text{s.t. } \boldsymbol{A}\boldsymbol{x} + \boldsymbol{B}\boldsymbol{w} + \boldsymbol{d}(\xi) \le \boldsymbol{0}\end{cases} \tag{23}$$

where $\boldsymbol{d}$ is the parameter vector, and the variation of $\boldsymbol{d}$ reveals uncertainty-induced disturbances in (9) and (11); ξ represents a random event or scenario that captures the uncertainty in model parameters; $\boldsymbol{x}$ is the vector of decision variables consisting of the output of generators and interruptible loads; $\boldsymbol{\kappa}$ is the vector of cost coefficients associated with $\boldsymbol{x}$; $\boldsymbol{w}$ is the vector of the optimization parameter symbolizing $[P_{TL,i,t}^{ab} \quad P_{TL,i,t+1}^{ab}]^{\mathrm{T}}$ and $[P_{TL,i,t}^{ab} \quad Z_t]^{\mathrm{T}}$; and $\boldsymbol{A}$ and $\boldsymbol{B}$ are the coefficient matrixes of $\boldsymbol{x}$ and $\boldsymbol{w}$, respectively. In this study, the robust transformation method in [24] is adopted to treat the uncertainty of renewable energy and interruptible load. As a popular model on uncertain optimal dispatch, robust optimization theory offers the advantages of not requiring a probability distribution and enabling fast calculation speeds, which is a suitable coping strategy for increasing the penetration of renewable energy integration [25].

First, the set of the uncertainty parameters $P_{RE,i,j,t}^{ACT}$ is constructed as shown in (24). Note that each uncertain factor is described in the form of intervals in which $\hat{P}_{RE,i,j,t}^{ACT}$ is constant.

$$P_{RE,i,j,t}^{ACT} \in [P_{RE,i,j,t}^{ACT} - \hat{P}_{RE,i,j,t}^{ACT}, P_{RE,i,j,t}^{ACT} + \hat{P}_{RE,i,j,t}^{ACT}] \tag{24}$$

Then, the original constraint (11) is transformed into constraint (25) by introducing auxiliary variables $\chi_{RE,i,j,t}$. Therefore, the stochastic elements in the vector $\boldsymbol{d}$ are transformed into the matrix $\boldsymbol{A}$. Equation (23) is rephrased as (26).

$$\begin{cases}\sum\limits_{j \in \Phi_{NRE,i}^a} P_{RE,i,j,t} - \sum\limits_{j \in \Phi_{NRE,i}^a} \{P_{RE,i,j,t}^{ACT}\} \chi_{RE,i,j,t} \le 0 & \forall i \in \Phi_{RE}^a \\ -1 \le \chi_{RE,i,j,t} \le 1 & \forall i \in \Phi_{RE}, \forall j \in \Phi_{NRE,i}^a\end{cases} \tag{25}$$

$$\begin{cases}\min z = \boldsymbol{\kappa}^{\mathrm{T}} \boldsymbol{x} \\ \text{s.t. } \boldsymbol{A}(\xi)\boldsymbol{x} + \boldsymbol{B}\boldsymbol{w} + \boldsymbol{d} \le \boldsymbol{0}\end{cases} \tag{26}$$

where $\Phi_{NRE,i}^a$ is the set of non-dispatchable renewable generation units at bus i in region a. Further, the robust method proposed by Bertsimas is employed in this study to solve (26) by transforming (25) into its standard robust equivalent form, as shown in (27).

$$\begin{cases}\sum\limits_{j \in \Phi_{NRE}^i} P_{RE,i,j,t} - \sum\limits_{j \in \Phi_{NRE}^i} P_{RE,i,j,t}^{ACT} \chi_{RE,i,j,t} + \\ \max\limits_{\{S_i \cup \tau_i | S_i \subseteq J_i, |S_i| = |\Gamma_i|, \tau_i \in J_i \setminus S_i\}} \left(\sum\limits_{j \in S_i} \hat{P}_{RE,i,j,t}^{ACT} y_j + \left(\Gamma_i - \lfloor \Gamma_i \rfloor \right) \hat{P}_{RE,i,\tau_i,t}^{ACT} y_{\tau_i} \right) \le 0 & \forall i \in \Phi_{RE} \\ -y_j \le \chi_{RE,i,j,t} \le y_j & \forall i \in \Phi_{RE}, \forall j \in \Phi_{NRE}^i\end{cases} \tag{27}$$

where y_j is an auxiliary variable; J_i is the set of uncertain parameters; and Γ_i is the robust conservatism budget coefficient that adjusts the conservatism of the model.

An uncertain problem given in (26) could be treated as a deterministic problem in terms of the constraint in (27). However, problems expressed in this form are still not solvable due to the bi-level nature of the optimization problem. Therefore, the duality theory allows (27) to be converted into (28) incorporating the auxiliary constraints in (29). Then, (26) can be compactly restated as (30). Detailed deduction can be referred to [26].

$$\sum_{j \in \Phi_{NRE}^i} P_{RE,i,j,t} - \sum_{j \in \Phi_{NRE}^i} P_{RE,i,j,t}^{ACT} \chi_{RE,i,j,t} + z_i \Gamma_i + \sum_{j \in J} P_{RE,i,j,t} \le 0 \quad \forall i \in \Phi_{RE} \tag{28}$$

$$\begin{cases} z_i + P_{RE,i,j,t} \ge \hat{P}_{RE,i,j,t}^{ACT} y_j & \forall i \in \Phi_{RE}, \forall j \in J \\ -y_j \le \chi_{RE,i,j,t} \le y_j & \forall i \in \Phi_{RE}, j \in \Phi_{NRE}^i \\ P_{RE,i,j,t} \ge 0 & \forall i \in \Phi_{RE}, \forall j \in \Phi_{NRE}^i \\ z_i \ge 0 & \forall i \in \Phi_{RE} \\ -1 \le \chi_{RE,i,j,t} \le 1 & \forall i \in \Phi_{RE}, \forall j \in \Phi_{NRE}^i \end{cases} \tag{29}$$

$$\begin{cases}\min z = \boldsymbol{\kappa}^{\mathrm{T}} \boldsymbol{x} \\ \text{s.t. } \boldsymbol{A}(\boldsymbol{\Gamma})\boldsymbol{x} + \boldsymbol{B}\boldsymbol{w} + \boldsymbol{d} \le \boldsymbol{0}\end{cases} \tag{30}$$

where $\boldsymbol{\Gamma}$ is the vector consisting of Γ_i.

The robust equivalence transformation refines the original uncertainty problem into a linear programming problem. Accordingly, this study provides a model packaging mechanism for the dispatch model by solving the feasible region of $\boldsymbol{w}$ based on multi-parameter programming theory. Firstly, the Lagrange function L is constructed in (31), and the optimality conditions for the problem in (30) are given as (32)-(34).

$$L=\boldsymbol{\kappa}^{\mathrm{T}}\boldsymbol{x}+\boldsymbol{u}^{\mathrm{T}}(\boldsymbol{A}(\boldsymbol{\Gamma})\boldsymbol{x}+\boldsymbol{B}\boldsymbol{w}+\boldsymbol{d}) \tag{31}$$

$$\nabla_x L=\boldsymbol{\kappa}+(\boldsymbol{A}(\boldsymbol{\Gamma}))^{\mathrm{T}}\boldsymbol{u}=\boldsymbol{0} \tag{32}$$

$$\mathrm{diag}(\boldsymbol{u})\cdot(\boldsymbol{A}(\boldsymbol{\Gamma})\boldsymbol{x}+\boldsymbol{B}\boldsymbol{w}+\boldsymbol{d})\le\boldsymbol{0} \tag{33}$$

$$\boldsymbol{u}\ge\boldsymbol{0} \tag{34}$$

where $\boldsymbol{u}$ is the vector of dual variables (Lagrange multipliers). Constraints in (30) can be classified into active and inactive constraints based on whether they reach the boundary or not, with the assumption that the solution is known. $\boldsymbol{A}$, $\boldsymbol{B}$, $\boldsymbol{d}$, and $\boldsymbol{u}$ are concisely expressed in vector forms as:

$$\begin{cases}\boldsymbol{A}(\boldsymbol{\Gamma})=((\boldsymbol{a}(\boldsymbol{\Gamma}))_i^{\mathrm{T}})_{i\in\tau}\\ \boldsymbol{B}=(\boldsymbol{b}_i^{\mathrm{T}})_{i\in\tau}\\ \boldsymbol{d}=(\boldsymbol{d}_i)_{i\in\tau}\\ \boldsymbol{u}=(\boldsymbol{u}_i)_{i\in\tau}\end{cases} \tag{35}$$

where τ is the set of constraints; $\boldsymbol{a}$ is the row vector of $\boldsymbol{A}$; and $\boldsymbol{b}$ is the row vector of $\boldsymbol{B}$. Therefore, the optimality conditions (32)-(34) can be restated as:

$$\tau'\cup\tau''=\tau \tag{36}$$

$$\boldsymbol{\kappa}+((\boldsymbol{a}(\boldsymbol{\Gamma}))_i)_{i\in\tau'}(\boldsymbol{u}_i)_{i\in\tau'}+((\boldsymbol{a}(\boldsymbol{\Gamma}))_j)_{j\in\tau''}(\boldsymbol{u}_j)_{j\in\tau''}=\boldsymbol{0} \tag{37}$$

$$((\boldsymbol{a}(\boldsymbol{\Gamma}))_i^{\mathrm{T}})_{i\in\tau'}\boldsymbol{x}+(\boldsymbol{b}_i^{\mathrm{T}})_{i\in\tau'}\boldsymbol{w}+(\boldsymbol{d}_i)_{i\in\tau'}=\boldsymbol{0} \tag{38}$$

$$(\boldsymbol{u}_i)_{i\in\tau'}\ge\boldsymbol{0} \tag{39}$$

$$((\boldsymbol{a}(\boldsymbol{\Gamma}))_j^{\mathrm{T}})_{j\in\tau''}\boldsymbol{x}+(\boldsymbol{b}_j^{\mathrm{T}})_{j\in\tau''}\boldsymbol{w}+(\boldsymbol{d}_j)_{j\in\tau''}<\boldsymbol{0} \tag{40}$$

$$(\boldsymbol{u}_j)_{j\in\tau''}=\boldsymbol{0} \tag{41}$$

where τ' and τ'' are the sets of active and inactive constraints, respectively. Relation (42) can be obtained based on the associative formulations of (37), (38), and (41).

$$\begin{cases}\boldsymbol{x}=(((\boldsymbol{a}(\boldsymbol{\Gamma}))_i^{\mathrm{T}})_{i\in\tau'})^{-1}(-(\boldsymbol{b}_i^{\mathrm{T}})_{i\in\tau'}\boldsymbol{w}-(\boldsymbol{d}_i)_{i\in\tau'})\\ (\boldsymbol{u}_i)_{i\in\tau'}=(((\boldsymbol{a}(\boldsymbol{\Gamma}))_i^{\mathrm{T}})_{i\in\tau'})^{-1}(-\boldsymbol{\kappa})\end{cases} \tag{42}$$

Under a particular partition of active and inactive constraints, or a given separation of τ' and τ'', one subset of the feasible region of $\boldsymbol{w}$ can be obtained by substituting (42) into (39) and (40), which is defined as *CR* [14] in (43).

$$CR(\tau',\tau'')=\{\boldsymbol{w}|(((\boldsymbol{a}(\boldsymbol{\Gamma}))_i)_{i\in\tau'})^{-1}(-\boldsymbol{\kappa})\ge\boldsymbol{0},((\boldsymbol{a}(\boldsymbol{\Gamma}))_j^{\mathrm{T}})_{j\in\tau''}((\boldsymbol{a}(\boldsymbol{\Gamma})_i^{\mathrm{T}})_{i\in\tau'})^{-1}(-(\boldsymbol{b}_i^{\mathrm{T}})_{i\in\tau'}\boldsymbol{w}-(\boldsymbol{d}_i)_{i\in\tau'})+(\boldsymbol{b}_j^{\mathrm{T}})_{j\in\tau''}\boldsymbol{w}+(\boldsymbol{d}_j)_{j\in\tau''}<\boldsymbol{0}\} \tag{43}$$

Meanwhile, $\boldsymbol{x}$ in each CR can be formulated as a function of $\boldsymbol{w}$. In other words, the inter-regional power transfer scheme within each control region, carried by tie-lines, exhibits a consistent linear mapping relation with the intra-regional adjustable resources. The solution of $\boldsymbol{x}$ is transformed into a deterministic problem depending on the value of $\boldsymbol{w}$ and the selection of CRs (or the validation of active and inactive constraints).

$$\boldsymbol{x}=(((\boldsymbol{a}(\boldsymbol{\Gamma}))_i^{\mathrm{T}})_{i\in\tau'})^{-1}(-(\boldsymbol{b}_i^{\mathrm{T}})_{i\in\tau'}\boldsymbol{w}-(\boldsymbol{d}_i)_{i\in\tau'})\quad\boldsymbol{w}\in CR(\tau',\tau'') \tag{44}$$

The PTFR and OCFR are composed of multiple CRs, and the feasible region of $\boldsymbol{w}$ is the union set of CRs formed by all active and inactive constraints:

$$FR=\bigcup_{\tau'\cup\tau''=\tau}CR(\tau',\tau'') \tag{45}$$

$|\Phi_A||\Phi_T-1|$ models in (17) and $|\Phi_A||\Phi_T|$ models in (21) are solved separately to obtain $FR^a_{PT,t}$ and $FR^a_{OC,t}$. As shown in Supplementary Material A Fig. SA1, assuming that the transfer power is $P^{ab*}_{TL,i,t}$, $FR^a_{PT,t}$ limits the lower bound $\underline{P}^{ab*}_{TL,i,t+1}$ and upper bound $\bar{P}^{ab*}_{TL,i,t+1}$ of the feasible range of the tie-line power at $t+1$. Furthermore, subject to the temporal coupling limitation at t, the tie-line transfer power is represented as $P^{ab}_{TL,i,t+1}$ with a practical lower bound of $\max(\underline{P}_{TL,i,t+1},\underline{P}^{ab*}_{TL,i,t+1})$ and a practical upper bound of $\min(\bar{P}_{TL,i,t+1},\bar{P}^{ab*}_{TL,i,t+1})$. The coupling is inevitable when multiple dispatch time periods are simultaneously considered, whereas decoupling could be achieved by quantifying the single-period $FR^a_{PT,t}$. Thus, the quantization of $FR^a_{PT,t}$ could be proceeded parallelly for different regions ($\forall a\in\Phi_A$) and time periods ($\forall t\in\Phi_T$). The operation cost generated by $P^{ab*}_{TL,i,t}$ is not merely caused by the existence of multiple resources within the region, but the lower bound of the $FR^a_{OC,t}$ must be obtained with the objective of optimal economy. $P^{ab*}_{TL,i,t}$ ($\forall t\in\Phi_T$) corresponds to the operation cost $f^{a*}_{1,t}$ ($\forall t\in\Phi_T$).

C. Dispatch Strategy Based on PTFR and OCFR

In this study, the proposed method is established and described in the form of two regions, i.e., $\Phi_A=\{a,b\}$, subject to the packaged model and inter-regional constraints (13)-(16). The inter-regional dispatch model can be expressed by (46) while both regions a and b are packaged depending on PTFR and OCFR, without the information of CRs.

$$\begin{cases}\min\sum_{\forall t\in\Phi_T}(Z^a_t+Z^b_t)\\ \text{s.t. }(P^{ab}_{TL,i,t},P^{ab}_{TL,i,t+1})\in FR^a_{PT,t} & \forall t\in\Phi_T\\ \quad(P^{ab}_{TL,i,t},Z^a_t)\in FR^a_{OC,t} & \forall t\in\Phi_T\\ \quad(P^{ba}_{TL,i,t},P^{ba}_{TL,i,t+1})\in FR^b_{PT,t} & \forall t\in\Phi_T\\ \quad(P^{ba}_{TL,i,t},Z^b_t)\in FR^b_{OC,t} & \forall t\in\Phi_T\\ \quad P^{ab}_{TL,i,t}=-P^{ba}_{TL,i,t} & \forall t\in\Phi_T\\ \quad(15)\text{-}(18) & \forall t\in\Phi_T\end{cases} \tag{46}$$

Since the packaged model presents only external properties described by the transmitted power, privacy protection of individual grids can be achieved. Private and sensitive information, including network parameters, nodal loads, cost functions of generators and interruptible loads [27], as well as $\boldsymbol{\Gamma}$, cannot be inferred merely from PTFR and OCFR.

The computation of (46) can be performed by either region a, region b, or a coordination layer. In particular, when region b is packaged and region a retains the original model, the inter-regional dispatch model can be expressed as (47). In this case, computation tasks of inter-regional dispatch strategies are performed by region a, whose model packaging process can be eliminated in some cases for accelerating the overall computation process.

$$\begin{cases} \min \sum_{\forall t \in \Phi_T} (f_t^a + Z_t^b) \\ \text{s.t. (3)-(12)} & \forall t \in \Phi_T \\ (P_{TL,i,t}^{ba}, P_{TL,i,t+1}^{ba}) \in FR_{PT,t}^b & \forall t \in \Phi_T \\ (P_{TL,i,t}^{ba}, Z_t^b) \in FR_{OC,t}^b & \forall t \in \Phi_T \\ P_{TL,i,t}^{ab} = -P_{TL,i,t}^{ba} & \forall t \in \Phi_T \\ \text{(13)-(16)} & \forall t \in \Phi_T \end{cases} \tag{47}$$

Assuming that the solution of (46) or (47) is $\boldsymbol{w}^*$, the separation of active and inactive constraints or τ', τ'' can be determined. The adjustable resource dispatch strategies are obtained based on the mapping relation of (44), which is demonstrated in Supplementary Material A Fig. SA2.

$$\boldsymbol{x}^* = (((\boldsymbol{a}(\boldsymbol{\Gamma}))_i^{\mathrm{T}})_{i \in \bar{\tau}})^{-1} (-(\boldsymbol{b}_i^{\mathrm{T}})_{i \in \bar{\tau}} \boldsymbol{w}^* - (\boldsymbol{d}_i)_{i \in \bar{\tau}}) \tag{48}$$

The diagram of the entire procedure is summarized in Supplementary Material A Fig. SA3. Note that the calculation of PTFR, OCFR, and CR for each region can be executed parallelly.

IV. Numerical Simulation

A. Critical and Feasible Region Verification

As shown in Fig. 2, two interconnected 3-bus test systems are used to verify the calculation process of CRs, feasible regions, and mapping relations. The parameters of lines, units, and tie-lines can be referred to [28]. The unit cost is a quadratic function, which is handled by the segmented linearization method proposed in [29], and the number of linear segments is 1.

Assuming that the transfer capacity of the tie-line is 50 MW and the dispatch time periods are $\Phi_T = \{1, 2\}$, the proposed method is used to solve the PTFR and mapping relation for power transfer in region 1, and the results of mapping relation are shown in Table I, where $P_{G,m,t}^1$ is the active power output of generator m in region 1 during time period t; and $P_{TL,1}^{12}$ and $P_{TL,2}^{12}$ are the active power transfer values (or tie-line power flows) on the first and second transmission lines connecting region 1 and region 2, respectively.

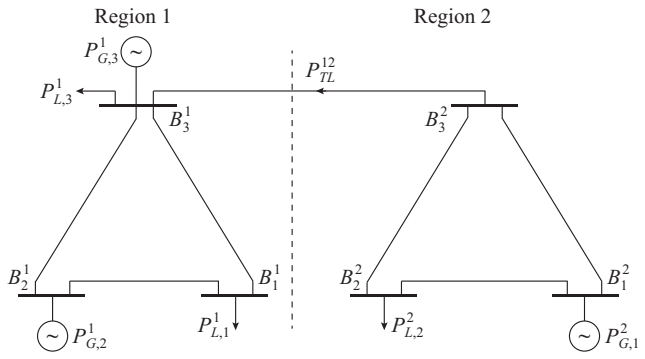

Fig. 2. Structure of two interconnected 3-bus test systems.

TABLE I
Results of Mapping Relation

CR	Region	Mapping relation
CR_1	$\left\{ \begin{bmatrix} P_{TL,1}^{12} \\ P_{TL,2}^{12} \end{bmatrix} \middle\| \begin{bmatrix} 0 & 1 \\ 0 & -1 \\ -1 & 0 \\ 1 & 0 \end{bmatrix} \begin{bmatrix} P_{TL,1}^{12} \\ P_{TL,2}^{12} \end{bmatrix} \le \begin{bmatrix} 30 \\ 0 \\ 0 \\ 45 \end{bmatrix} \right\}$	$\begin{bmatrix} P_{G,2,1}^1 \\ P_{G,2,2}^1 \\ P_{G,3,1}^1 \\ P_{G,3,2}^1 \end{bmatrix} = \begin{bmatrix} -1 & 0 \\ 0 & 0 \\ 0 & 0 \\ 0 & -1 \end{bmatrix} \begin{bmatrix} P_{TL,1}^{12} \\ P_{TL,2}^{12} \end{bmatrix} + \begin{bmatrix} 100 \\ 10 \\ 110 \\ 40 \end{bmatrix}$
CR_2	$\left\{ \begin{bmatrix} P_{TL,1}^{12} \\ P_{TL,2}^{12} \end{bmatrix} \middle\| \begin{bmatrix} 1 & 0 \\ 0 & 1 \\ -1 & 0 \\ 0 & -1 \\ 0.7 & -0.7 \end{bmatrix} \begin{bmatrix} P_{TL,1}^{12} \\ P_{TL,2}^{12} \end{bmatrix} \le \begin{bmatrix} 50 \\ 50 \\ 0 \\ -30 \\ 10.6 \end{bmatrix} \right\}$	$\begin{bmatrix} P_{G,2,1}^1 \\ P_{G,2,2}^1 \\ P_{G,3,1}^1 \\ P_{G,3,2}^1 \end{bmatrix} = \begin{bmatrix} -1 & 0 \\ 0 & 0 \\ 0 & -1 \\ 0 & 0 \end{bmatrix} \begin{bmatrix} P_{TL,1}^{12} \\ P_{TL,2}^{12} \end{bmatrix} + \begin{bmatrix} 100 \\ 10 \\ 140 \\ 10 \end{bmatrix}$
CR_3	$\left\{ \begin{bmatrix} P_{TL,1}^{12} \\ P_{TL,2}^{12} \end{bmatrix} \middle\| \begin{bmatrix} -0.7 & 0.7 \\ 1 & 0 \\ 0 & -1 \\ -1 & 0 \end{bmatrix} \begin{bmatrix} P_{TL,1}^{12} \\ P_{TL,2}^{12} \end{bmatrix} \le \begin{bmatrix} -10.6 \\ 50 \\ 0 \\ -45 \end{bmatrix} \right\}$	$\begin{bmatrix} P_{G,2,1}^1 \\ P_{G,2,2}^1 \\ P_{G,3,1}^1 \\ P_{G,3,2}^1 \end{bmatrix} = \begin{bmatrix} -1 & 0 \\ 0 & 0 \\ -1 & 0 \\ 1 & -1 \end{bmatrix} \begin{bmatrix} P_{TL,1}^{12} \\ P_{TL,2}^{12} \end{bmatrix} + \begin{bmatrix} 100 \\ 10 \\ 155 \\ -5 \end{bmatrix}$

Note: PTFR is the union set of all CRs.

In the inter-regional dispatch process, only PTFR and OCFR are needed. Equation (49) and Table I demonstrate how PTFR (marked as FR_{PT}) is calculated, and the intra-regional information will not be exposed. After the active power transfer scheme (i. e., the optimal solution of $P_{TL,1}^{12}$, $P_{TL,2}^{12}$, marked as $[P_{TL,1}^{12*}, P_{TL,2}^{12*}]^{\mathrm{T}}$ is decided, the CR to which the scheme belongs can be determined, and the intra-regional dispatch strategy can be obtained quickly based on mapping relation.

$$FR_{PT} = CR_1 \cup CR_2 \cup CR_3 = \left\{ \begin{bmatrix} P_{TL,1}^{12} \\ P_{TL,2}^{12} \end{bmatrix} \middle\| \begin{bmatrix} 1 & 0 \\ 0 & -1 \\ 0 & 1 \\ -1 & 0 \end{bmatrix} \begin{bmatrix} P_{TL,1}^{12} \\ P_{TL,2}^{12} \end{bmatrix} \le \begin{bmatrix} 50 \\ 0 \\ 50 \\ 0 \end{bmatrix} \right\} \tag{49}$$

In addition, a wind farm is supplemented at bus B_2^2. The forecast error is set to be 0.1, the component of $\boldsymbol{\Gamma}$ (i.e., Γ) is set to be 0.5, the number of linear segments is set to be 1, and the transfer capacity of the tie-line is set to be 100 MW.

The active power transfer and overall cost for different feasible regions of the tie-line are shown in Fig. 3, where the blocks with diverse colors represent different CRs.

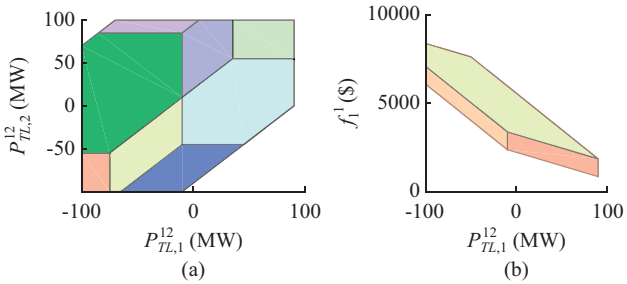

Fig. 3. Active power transfer and overall cost for different feasible regions of tie-line. (a) PTFR. (b) OCFR.

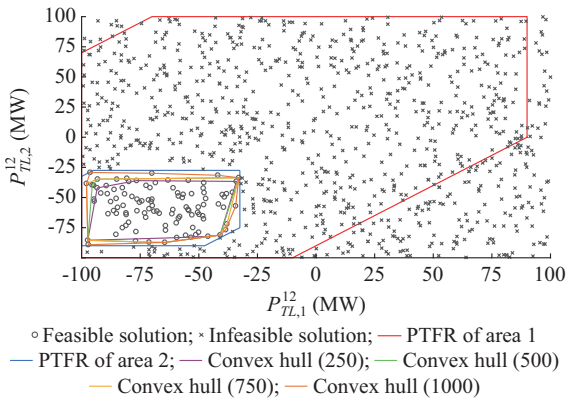

Fig. 4. Feasible region verification.

All the CRs are convex and disjoint, and the PTFR is formed by the outer boundaries. The tie-line transfer power does not always reach the maximum limit of 100 MW subject to the limitations of the line capacity and unit capacity. Due to the limited ramping capability of the unit, the adjustment margin of the tie-line transfer power at $t=2$ is affected by the tie-line transfer power at $t=1$. For example, when the tie-line transfer power is 45 MW at $t=1$, the tie-line transfer power at $t=2$ can be adjusted within (−45 MW, 100 MW). However, when the tie-line transfer power grows to 90 MW at $t=1$, the adjustable range of tie-line transfer power at $t=2$ is (0, 100 MW). Fixed tie-line transfer power is not mapped to a unique solution of adjustable resources within each region, resulting in differences in dispatch costs required for the same transfer power. However, with the object of minimizing cost, there exists a unique dispatch solution since the OCFR will adopt the lower bound.

Figure 4 presents the feasible region verification. Note that there is only one unit inside region 2, and accordingly, its PTFR range is smaller. Although the PTFR of the tie-line receiving end (region 1) is broader, the capacity of the tie-line sending end (region 2) is restricted, and the actual PTFR of the tie-line is the PTFR intersection of the sending- and receiving-end regions. To test the correctness of PTFR result, 250, 500, 750, and 1000 tie-line dispatch scenarios are randomly simulated, recording the feasibility of solutions, and convex hulls of feasible solutions are plotted. All infeasible solutions are located outside the PTFR, and with the increasing scale of stochastic simulation dispatch strategies, the convex hull boundaries formed by the feasible solutions gradually converge to the boundaries of the PTFR, which verifies that the model packaging mechanism can accurately identify the PTFR.

By setting Γ from 0 to 0.8, PTFR and OCFR are quantified, as demonstrated in Fig. 5. By comparing the results, it can be found that as the conservatism budget increases, the boundary of the feasible region gradually shrinks inward, and the range of the feasible region becomes smaller, leading to more conservative dispatch results, so as to improve the overall security of the system. Dispatchers can evade the potential impacts of stochasticity by adjusting Γ.

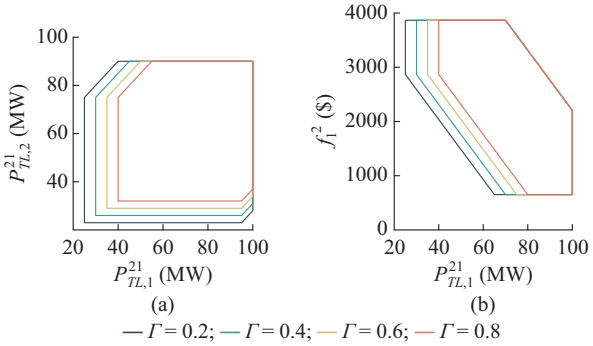

Fig. 5. Active power transfer and overall cost for different feasible regions with different degrees of Γ. (a) PTFR. (b) OCFR.

By defining the ramping rate as $R_R=P^a_{Gup,i}/\bar{P}^a_{G,i,t}$, PTFR with different ramping rates from 0.1 to 0.8 is shown in Fig. 6(a)-(h), respectively. With increasing ramping rates, the adjustment range of the unit output becomes wider, and the adjustable range of tie-line power during the adjacent time periods is correspondingly larger.

The number of linear segments of the unit cost function is assumed to be 1 in all previous studies, which does not lead to significant errors but improves the efficiency of solving the model. To study the impact of diverse number of linear segments in Fig. 7, all CRs are quantified and counted with the number of linear segments ranging from 1 to 10.

The number of CRs increases significantly along with the number of linear segments. Each CR needs to be explored and a mapping relation is established with the intra-regional resources, thus increasing the model complexity and computation burden. Furthermore, the JED is solved based on the traditional centralized method and the proposed method, respectively. The results show that the errors of the two methods are less than 10^{-4} for different numbers of linear segments. When linear segment number is set to be 10 as a reference, the error is the largest at $a=1$, which is 0.497%. When the number of linear segments increases to 2, the error rapidly decreases to 0.088%. The calculation error is not significantly reduced for the further increase of linear segment. However, the total number of CRs is increased by 53.19% when the number of linear segments is 2 as compared with 1.

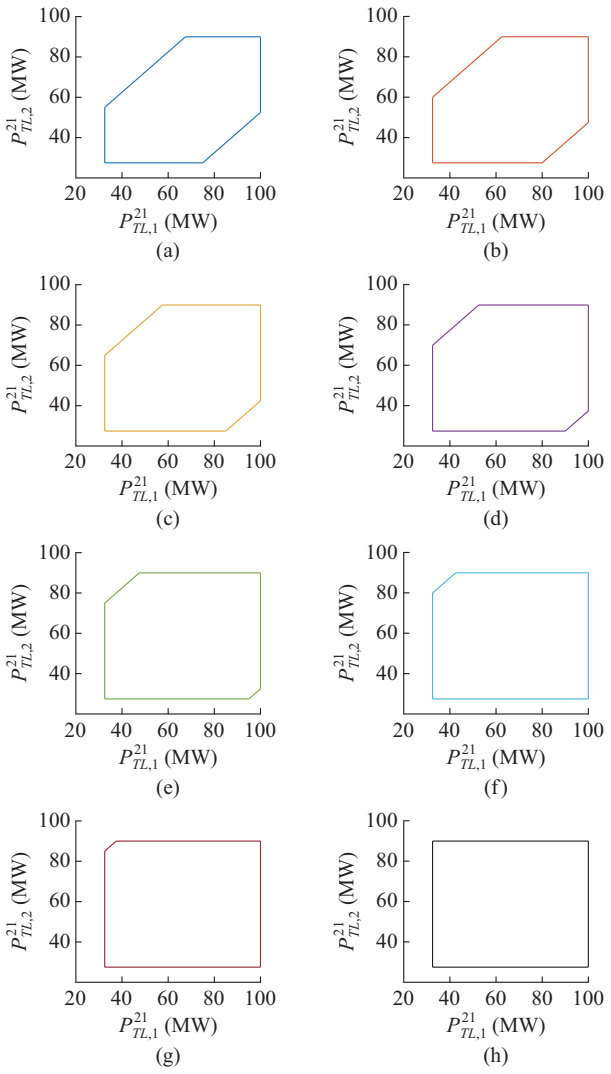

Fig. 6. PTFR with different ramping rates. (a) R_R=0.1. (b) R_R=0.2. (c) R_R=0.3. (d) R_R=0.4. (e) R_R=0.5. (f) R_R=0.6. (g) R_R=0.7. (h) R_R=0.8.

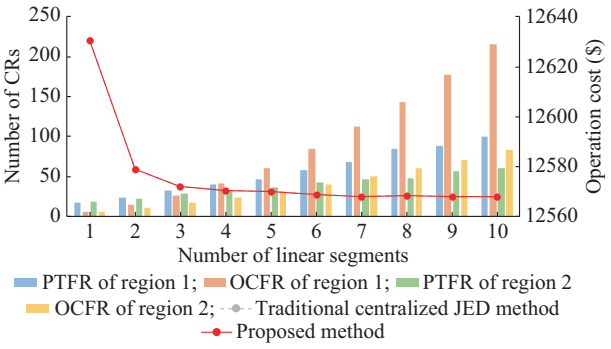

Fig. 7. Results with different number of linear segments.

B. Analysis of Dispatch Result

For modified IEEE 30-bus and 14-bus test systems shown in Fig. 8, the power transfer scheme is solved based on the proposed method, whose results are compared with traditional centralized JED method. The tie-line connects bus 14 of IEEE 30-bus test system and bus 9 of IEEE 14-bus test system with the maximum transfer capacity being 100 MW. The IEEE 14-bus test system contains 3 photovoltaic farms and 3 wind farms, while the IEEE 30-bus test system possesses 7 photovoltaic farms and 7 wind farms. The capacity of each photovoltaic farm and wind farm is 25 MW. Meanwhile, generators at buses 3, 6, and 8 of IEEE 14-bus test system and buses 5 and 11 of IEEE 30-bus test system are eliminated. The renewable energy output is set to fluctuate within the range of 90% and 110% of the forecast value. PD^{ab}_{TL} and PU^{ab}_{TL} are set to be −50 MW and 50 MW, respectively. σ is set to be 0.5, and P^{ab}_{TL} is set to be 720 MW.

As shown in Fig. 9, based on the proposed method and traditional centralized JED method, results under different Γ are obtained, where the proposed method contains two forms, one for multi-region equivalence method shown in (46), and the other for the single-region equivalence method demonstrated in (47). By using the results of traditional centralized JED method as a reference, the errors of both methods are small, which verifies the correctness of the proposed method. However, as shown in Fig. 10, the calculation time required when using the multi-region equivalence method is significantly shorter than that using the traditional centralized JED method. With a fixed Γ of 0.1, the generator outputs under the three methods are shown in Fig. 11, where the generator output is consistent despite the difference of solving methods. In Fig. 11, generators G1-G4 are connected to buses 1, 2, 8, and 13 of region 2, respectively, and G5 and G6 are connected to buses 1 and 2 of region 1, respectively.

To study how tie-line regulation parameters influence power transfer performance, the ramping rate $R_{TLR}=PU^{ab}_{TL}/\bar{P}^{ab}_{TLi}$, σ, and the total transfer power rate $R_{TTP}=P^{ab}_{TL}/P^{ab*}_{TL}$ are adjusted, respectively, and the analysis of inter-regional dispatch results is shown in Fig. 12. As a benchmark of this subsection, R_{TLR} is initialized to be 0.05, and σ is set to be 0.5, while the total transfer power is 720 MW, First, R_{TLR} grows from 0.01 to 0.09, and the analysis of inter-regional dispatch results is shown in Fig. 12. As R_{TLR} decreases, the transfer power gradually stabilizes and simultaneously, the dispatch cost increases. Smaller value of tie-line fluctuation rate σ leads to more stable tie-line power transfer but extra dispatch cost. Furthermore, the overall dispatch cost decreases along with the increase of R_{TTP}, but the reduction slows down when R_{TTP} exceeds 1.1.

C. Verification of Generalization Capability

In this subsection, we randomly connect 5, 10, 15, ..., and 50 nodes of IEEE 14-bus test system to the IEEE 118-bus test system as an interconnected grid to demonstrate the computation performance under upgrowing system scale. Each IEEE 14-bus test system contains 6 renewable energy and 3 interruptible loads. Locations of the sending and receiving ends of each tie-line, and the integration positions of renewable energy sources as well as interruptible loads, are all generated in a stochastic way. By setting the number of cores for parallel execution to be 10 and time consumption limit to be 36000 s, the computation time with varying number of regions of the proposed method and the traditional centralized JED method is shown in Fig. 13.

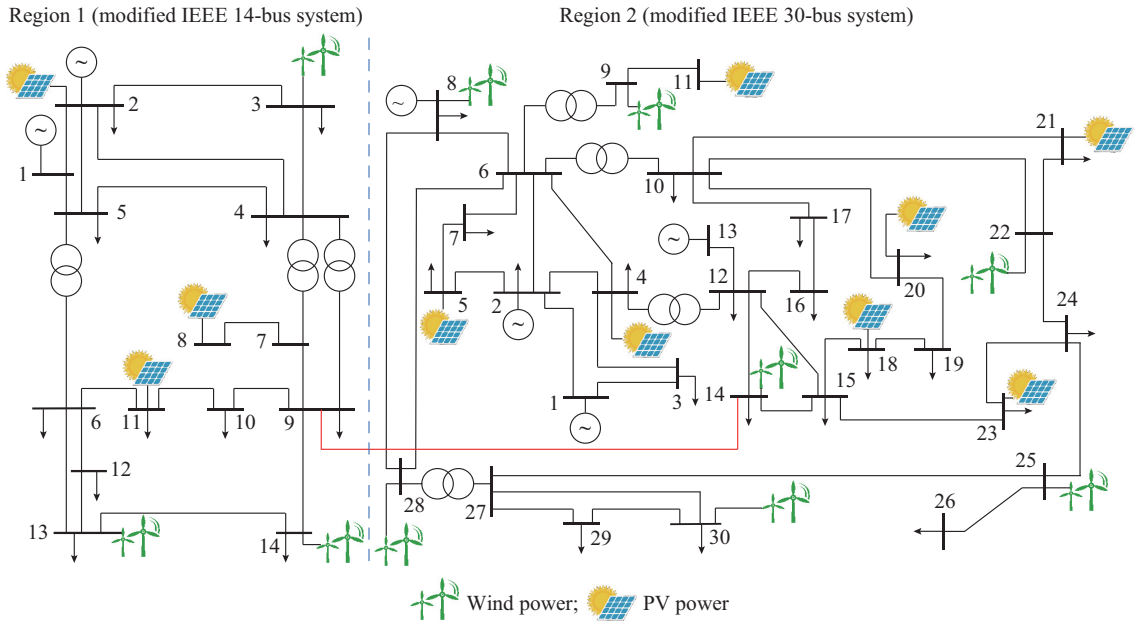

Fig. 8. Modified IEEE 30-bus and 14-bus test systems.

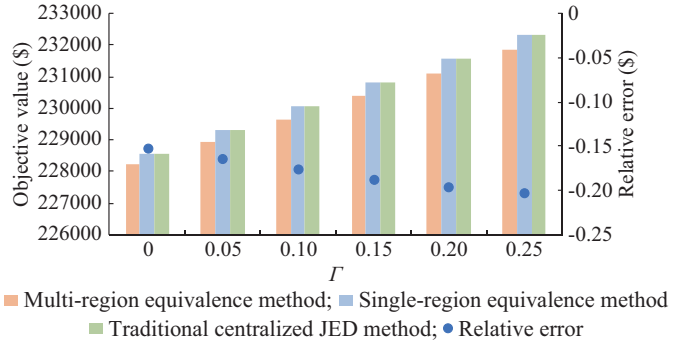

Fig. 9. Comparison of dispatch results.

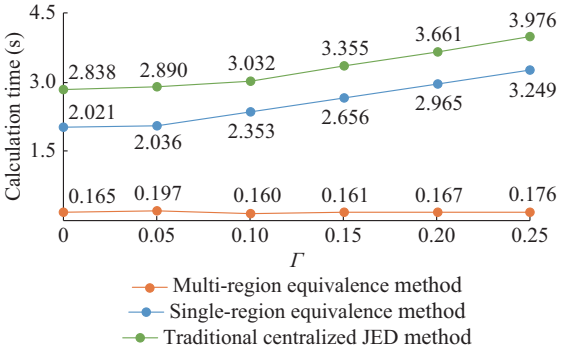

Fig. 10. Comparison of calculation time.

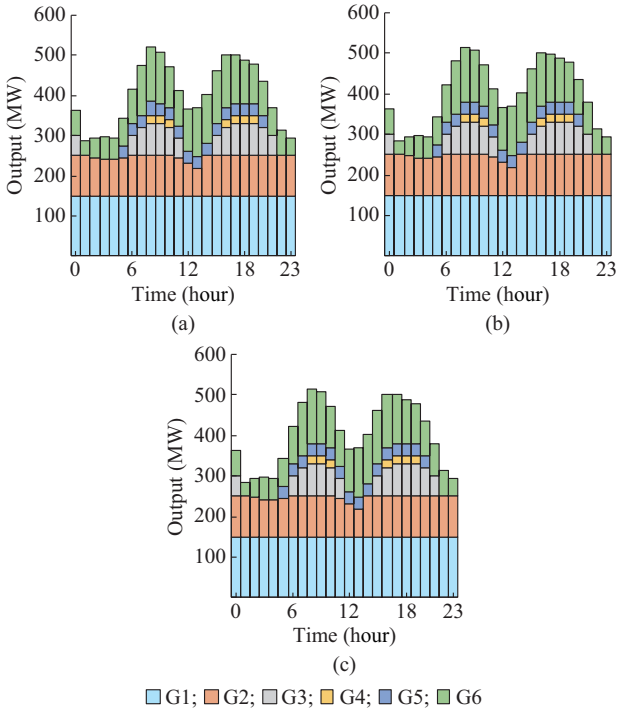

Fig. 11. Comparison of generator outputs under three methods. (a) Multi-region equivalence method. (b) Single-region equivalence method. (c) Traditional centralized JED method.

When the number of regions is less than 25, both methods can complete the solution. The proposed method spends time mainly on the model packaging process. Consequently, when the number of regions is 5, the total calculation time of the proposed method is 28.25% higher than that of the traditional centralized JED method. However, when the number of regions increases to 10-25, the total calculation time required by the proposed method is only 8.84%-49.00% of that of the traditional centralized JED method.

The proposed method is more time-saving for systems with numerous regions, although the scale of each region is recommended to be moderate to avoid model degeneracy due to excessive time consumption on model packaging. When the number of regions is greater than 25, the traditional centralized JED method is unable to complete the task under a centralized method, whereas both the packaging and calculation time of the proposed method grow linearly, completing the computation with significantly higher efficiency.

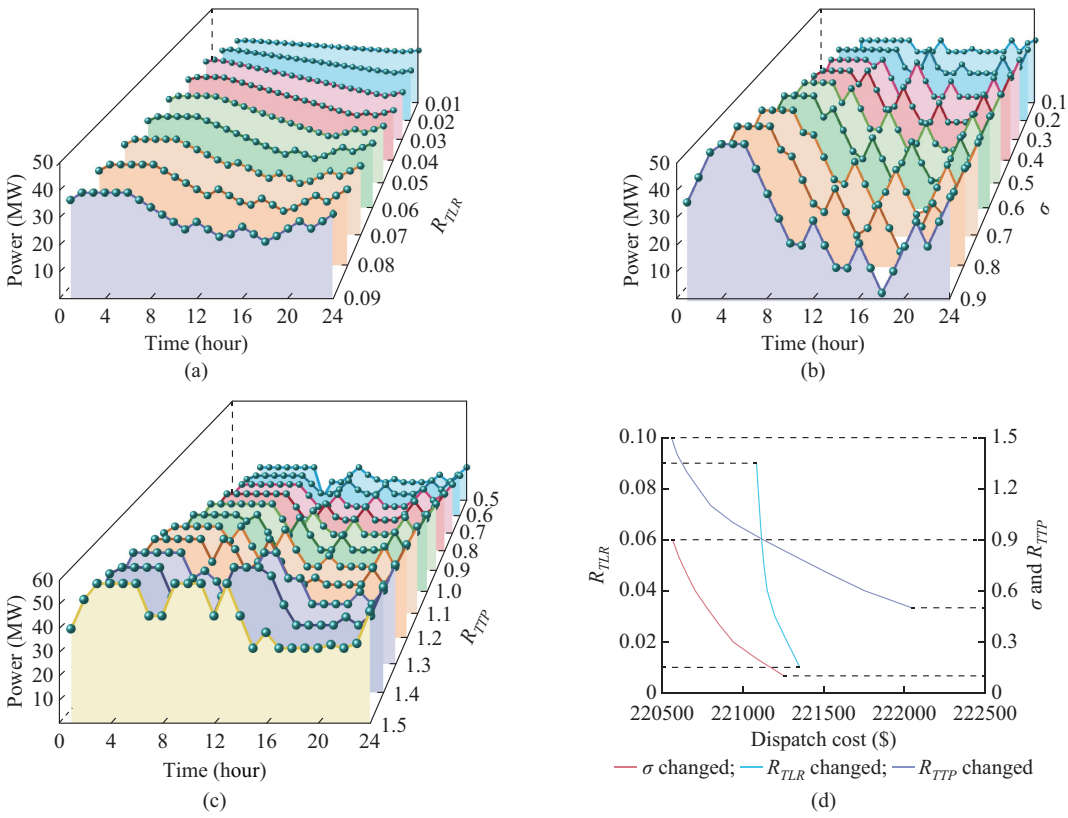

Fig. 12. Analysis of inter-regional dispatch results. (a) Results with varying ramping rate. (b) Results with varying fluctuation rate. (c) Results with varying total transfer power rate. (d) Comparison of dispatch cost.

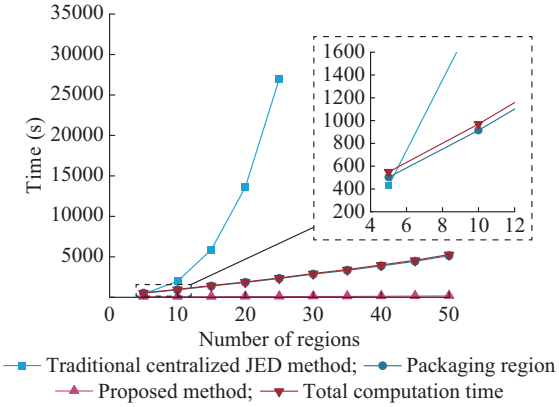

Fig. 13. Computation time with varying number of regions of proposed method and traditional centralized JED method.

For industrial application scenarios, the model packaging process is executed by the independent operators in each region, where the number of parallel cores is not restricted, and the efficiency of the proposed method can be further improved compared with the numerical simulation above.

V. Conclusion

In this study, a non-iterative robust economic dispatch method is proposed, which can accomplish the coordinated dispatch of interconnected grids under high percentage of renewable energy integration, and simultaneously protect the intra-regional private information. Each grid is packaged as an equivalent model containing CR, PTFR, and OCFR. The packaging process can be performed in parallel by temporal and spatial decomposition. Inter-regional dispatch strategies can be accomplished based on PTFR and OCFR. Γ can adjust the boundaries of feasible regions to address the risk of stochasticity. Mapping relations between inter-regional power transfer schemes and intra-regional adjustable resources in each CR accelerates the solution of the intra-regional economic dispatch. The proposed method has some limitations. Voltage constraints and reactive power output of generators are eliminated to ensure the JED model explicitly and linearly, and the expansion to active and reactive power coordination is an important topic for our future work.

References

[1] H. Gao, T. Jin, G. Wang *et al*., "Low-carbon dispatching for virtual power plant with aggregated distributed energy storage considering spatiotemporal distribution of cleanness value," *Journal of Modern Power Systems and Clean Energy*, vol. 12, no. 2, pp. 346-358, Mar. 2024.

[2] N. Zhang, J. Cheng, and Y. Wang, "Probabilistic optimal energy flow of district multienergy systems: an MPLP-based online dictionary-learning approach," *IEEE Transactions on Industrial Informatics*, vol. 15, no. 9, pp. 4867-4877, Sept. 2019.

[3] Z. Zhuo, N. Zhang, J. Yang *et al*., "Transmission expansion planning test system for AC/DC hybrid grid with high variable renewable energy penetration," *IEEE Transactions on Power Systems*, vol. 35, no. 4, pp. 2597-2608, Jul. 2020.

[4] H. Zhong, Q. Xia, C. Kang *et al*., "An efficient decomposition method for the integrated dispatch of generation and load," *IEEE Transactions on Power Systems*, vol. 30, no. 6, pp. 2923-2933, Nov. 2015.

[5] X. Dong, X. Hao, Q. Chen *et al*., "A distributed power transfer limit calculation method for multi-area interconnection power networks," *IEEE Transactions on Power Systems*, vol. 36, no. 5, pp. 4723-4732,

Sept. 2021.
[6] X. Dong, H. Sun, C. Wang *et al*., "Power flow analysis considering automatic generation control for multi-area interconnection power networks," *IEEE Transactions on Industry Applications*, vol. 53, no. 6, pp. 5200-5208, Nov. 2017.
[7] H. Guo, Q. Chen, Y. Gu *et al*., "A data-driven pattern extraction method for analyzing bidding behaviors in power markets," *IEEE Transactions on Smart Grid*, vol. 11, no. 4, pp. 3509-3521, Jul. 2020.
[8] M. White and R. Pike. (2011, Jan.). ISO New England and New York ISO interregional interchange scheduling: analysis and options. [Online]. Available: https://www.iso-ne.com/pubs/whtpprs/iris_white_paper.pdf.
[9] Y. Xue, Z. Li, C. Lin *et al*., "Coordinated dispatch of integrated electric and district heating systems using heterogeneous decomposition," *IEEE Transactions on Sustainable Energy*, vol. 11, no. 3, pp. 1495-1507, Jul. 2020.
[10] Z. Li, Q. Guo, H. Sun *et al*., "Coordinated transmission and distribution AC optimal power flow," *IEEE Transactions on Smart Grid*, vol. 9, no. 2, pp. 1228-1240, Mar. 2018.
[11] J. Wang, H. Zhong, Z. Yang *et al*., "Incentive mechanism for clearing energy and reserve markets in multi-area power systems," *IEEE Transactions on Sustainable Energy*, vol. 11, no. 4, pp. 2470-2482, Oct. 2020.
[12] J. Wang, H. Zhong, Z. Ma *et al*., "Review and prospect of integrated demand response in the multi-energy system," *Applied Energy*, vol. 202, pp. 772-782, Sept. 2017.
[13] Y. Ju, Z. Zhang, W. Wu *et al*., "A bi-level consensus ADMM-based fully distributed inverter-based volt/var control method for active distribution networks," *IEEE Transactions on Power Systems*, vol. 37, no. 1, pp. 476-487, Jan. 2022.
[14] Y. Guo, L. Tong, W. Wu *et al*., "Coordinated multi-area economic dispatch via critical region projection," *IEEE Transactions on Power Systems*, vol. 32, no. 5, pp. 3736-3746, Sept. 2017.
[15] S. Liu, Z. Yang, Q. Xia *et al*., "Power trading region considering long-term contract for interconnected power networks," *Applied Energy*, vol. 261, p. 114411, Mar. 2020.
[16] W. Lin, Z. Yang, J. Yu *et al*., "Tie-line security region considering time coupling," *IEEE Transactions on Power Systems*, vol. 36, no. 2, pp. 1274-1284, Mar. 2021.
[17] W. Lin, Z. Yang, J. Yu *et al*., "Determination of transfer capacity region of tie lines in electricity markets: theory and analysis," *Applied Energy*, vol. 239, pp. 1441-1458, Apr. 2019.
[18] W. Lin, Z. Yang, J. Yu *et al*., "Tie-line power transmission region in a hybrid grid: fast characterization and expansion strategy," *IEEE Transactions on Power Systems*, vol. 35, no. 3, pp. 2222-2231, May 2020.
[19] Z. Tan, H. Zhong, Q. Xia *et al*., "Non-iterative multi-area coordinated dispatch via condensed system representation," *IEEE Transactions on Power Systems*, vol. 36, no. 2, pp. 1594-1604, Mar. 2021.
[20] Z. Tan, H. Zhong, J. Wang *et al*., "Enforcing intra-regional constraints in tie-line scheduling: a projection-based framework," *IEEE Transactions on Power Systems*, vol. 34, no. 6, pp. 4751-4761, Nov. 2019.
[21] W. Dai, Z. Yang, J. Yu *et al*., "Economic dispatch of interconnected networks considering hidden flexibility," *Energy*, vol. 223, p. 120054, May 2021.
[22] Y. Ju, J. Wang, F. Ge *et al*., "Unit commitment accommodating large scale green power," *Applied Sciences*, vol. 9, no. 8, p. 1611, Apr. 2019.
[23] X. Chen, J. Lv, M. B. McElroy *et al*., "Power system capacity expansion under higher penetration of renewables considering flexibility constraints and low carbon policies," *IEEE Transactions on Power Systems*, vol. 33, no. 6, pp. 6240-6253, Nov. 2018.
[24] Y. Hou, M. Bao, and Y. Ding, "Bi-level robust clearing framework of integrated electricity and gas market considering robust bidding of smart energy hubs," *Journal of Modern Power Systems and Clean Energy*, vol. 13, no. 1, pp. 351-364, Jan. 2025.
[25] Y. Ma, X. Dong, X. Yang *et al*., "Robust optimization model of AC/DC hybrid distribution network considering renewable energy uncertainty," in *Proceedings of 2022 4th International Conference on Smart Power & Internet Energy Systems*, Beijing, China, Dec. 2022, pp. 679-684.
[26] D. Bertsimas and M. Sim, "The price of robustness," *Operations Research*, vol. 52, no. 1, pp. 35-53, Jan. 2004.
[27] Z. Tan, Z. Yan, H. Zhong *et al*., "Non-iterative solution for coordinated optimal dispatch via equivalent projection – part I: theory," *IEEE Transactions on Power Systems*, vol. 39, no. 1, pp. 890-898, Jan. 2024.
[28] A. Kargarian, Y. Fu, and Z. Li, "Distributed security-constrained unit commitment for large-scale power systems," *IEEE Transactions on Power Systems*, vol. 30, no. 4, pp. 1925-1936, Jul. 2015.
[29] M. Carrion and J. M. Arroyo, "A computationally efficient mixed-integer linear formulation for the thermal unit commitment problem," *IEEE Transactions on Power Systems*, vol. 21, no. 3, pp. 1371-1378, Aug. 2006.

Yuejian Wu received the B.S. degree in electrical engineering from Shandong University, Jinan, China, in 2023. He is currently pursuing the M.S. degree at Shandong University. His research interests include power system stability and operation.

Xiaoming Dong received the B.S., M.S., and Ph.D. degrees in electrical engineering from Shandong University, Jinan, China, in 2003, 2009, and 2013, respectively. He is currently an Associate Professor of Shandong University. His research interests include power system stability, operation, and control.

Tianguang Lu received the B.S. degree in electrical engineering from Shandong University, Jinan, China, in 2013, and the Ph.D. degree in electrical engineering from Shanghai Jiao Tong University, Shanghai, China, in 2018. He is currently a Professor of Shandong University. His research interests include power distribution system, microgrid, intelligent algorithm, and renewable energy.

Zhengqi Liu received the B.S. degree in electrical engineering from Wuhan University of Technology, Wuhan, China, in 2021, and the M.S. degree in electrical engineering from Shandong University, Jinan, China, in 2024. He is currently an Engineer of State Grid Changsha Power Supply Company, Changsha, China. His research interests include power system stability and operation.

Chengfu Wang received the B. S. degree in electrical engineering from Northeast Electric Power University, Jilin, China, in 2006, the M.S. degree in electrical engineering from Harbin Institute of Technology, Harbin, China, in 2008, and the Ph.D. degree from Shandong University, Jinan, China, in 2012. He is currently an Associate Professor of Shandong University. His research interest includes integrated energy system planning and operation.